SUPPLEMENTARY MATERIAL

"IMPLICATIONS OF LONGITUDINAL RIDGES FOR THE MECHANICS OF ICE-FREE LONG RUNOUT LANDSLIDES."

by Magnarini et al.

Supplementary Table T1 – Details of planned drone flight paths.

Flight plan area	N° images	Altitude	Camera Angle	Frontal Overlap	Lateral overlap
Distal Lobes (Supplementary Figure S3b)	290	150 m	90°	65%	65%
Proximal Lobes (Supplementary Figure S3c	134	250 m	90°	65%	65%

Supplementary Table T2 – List of Ground Control Points (GCPs) used to georeference drone-derived digital elevation models. Locations of GCPs are shown in Supplementary Figure S3a.

GCP Name on map	Latitude	Longitude	Grid Zone	Easting	Northing	Altitude (m)	Notes
GCP1	20º 27' 10.3260" S	70º 08' 41.7315" W	19K	380575	7737986	66.068	
GCP2	20º 27' 11.1127" S	70º 08' 45.7404" W	19K	380459	7737961	71.386	
GCP3	20º 27' 17.7846" S	70º 08' 54.9696" W	19K	380193	7737754	69.481	
GCP4	20º 27' 27.5261" S	70º 09' 02.3238" W	19K	379982	7737453	78.366	
GCP5	20º 27' 30.0692" S	70º 09' 01.4109" W	19K	380009	7737375	78.146	
GCP6	20º 27' 41.1022" S	70º 08' 50.5184" W	19K	380327	7737038	51.862	
GCP7	20º 27' 45.5253" S	70º 09' 00.4217" W	19K	380041	7736900	77.414	
GCP8	20º 27' 30.6623" S	70º 08' 45.4713" W	19K	380471	7737360	57.792	
GCP9	20º 27' 18.5647" S	70º 08' 40.2396" W	19K	380620	7737733	55.155	Not in this work
GCP10	20º 27' 48.5090" S	70º 08' 42.0145" W	19K	380575	7736812	59.44	Not in this work
GCP11	20º 27' 28.1983" S	70º 08' 34.3751" W	19K	380792	7737438	54.788	Not in this work
GCP12	20º 27' 37.0776" S	70º 08' 34.4063" W	19K	380793	7737165	60.352	Not in this work
GCP13	20º 27' 13.0662" S	70º 08' 30.6051" W	19K	380898	7737904	58.748	Not in this work
GCP14	20º 27' 14.7146" S	70º 08' 27.2353" W	19K	380996	7737854	60.634	
GCP15	20º 27' 24.9899" S	70º 08' 27.6563" W	19K	380986	7737538	57.608	
GCP16	20º 27' 28.4871" S	70º 08' 25.0593" W	19K	381062	7737431	58.11	
GCP17	20º 27' 38.9129" S	70º 08' 22.3753" W	19K	381142	7737111	102.349	
GCP18	20º 27' 15.2138" S	70º 08' 10.6052" W	19K	381478	7737842	92.502	
GCP19	20º 27' 48.4800" S	70º 06' 51.3338" W	19K	383782	7736835	804.74	
GCP20	20º 27' 35.3179" S	70º 06' 49.6513" W	19K	383828	7737240	795.492	Not in this work
GCP21	20º 27' 30.0692" S	70º 09' 01.4109" W	19K	380575	7737986	66.068	Not in this work

Supplementary Table 3 – Error estimation of the reconstructed coastal plain surface underneath the landslide deposit. Standard deviation of the topographic elevation measurements along each set of transects and propagation of error, as derived from the equation $\sigma_k = \sqrt{\sigma_i^2 + \sigma_j^2}$, to evaluate errors on the deposit thickness calculation for Lobe 1, 2, and 3 (error bars in Figure 3b in the main manuscript).

Sets of Profiles	Standard Deviation σ	Propagation of error σ_k
Yellow line 1	1.51 (σ_i)	3.48 (Lobe 1)
Yellow line 2	3.13 (σ_j)	
Yellow line 3	2.04 (σ_i)	2.27 (Lobe 2)
Yellow line 4	1.01 (σ_j)	
Yellow line 5	8.3 (σ_i)	8.61 (Lobe 3)
Yellow line 6	3.3 (σ_j)	

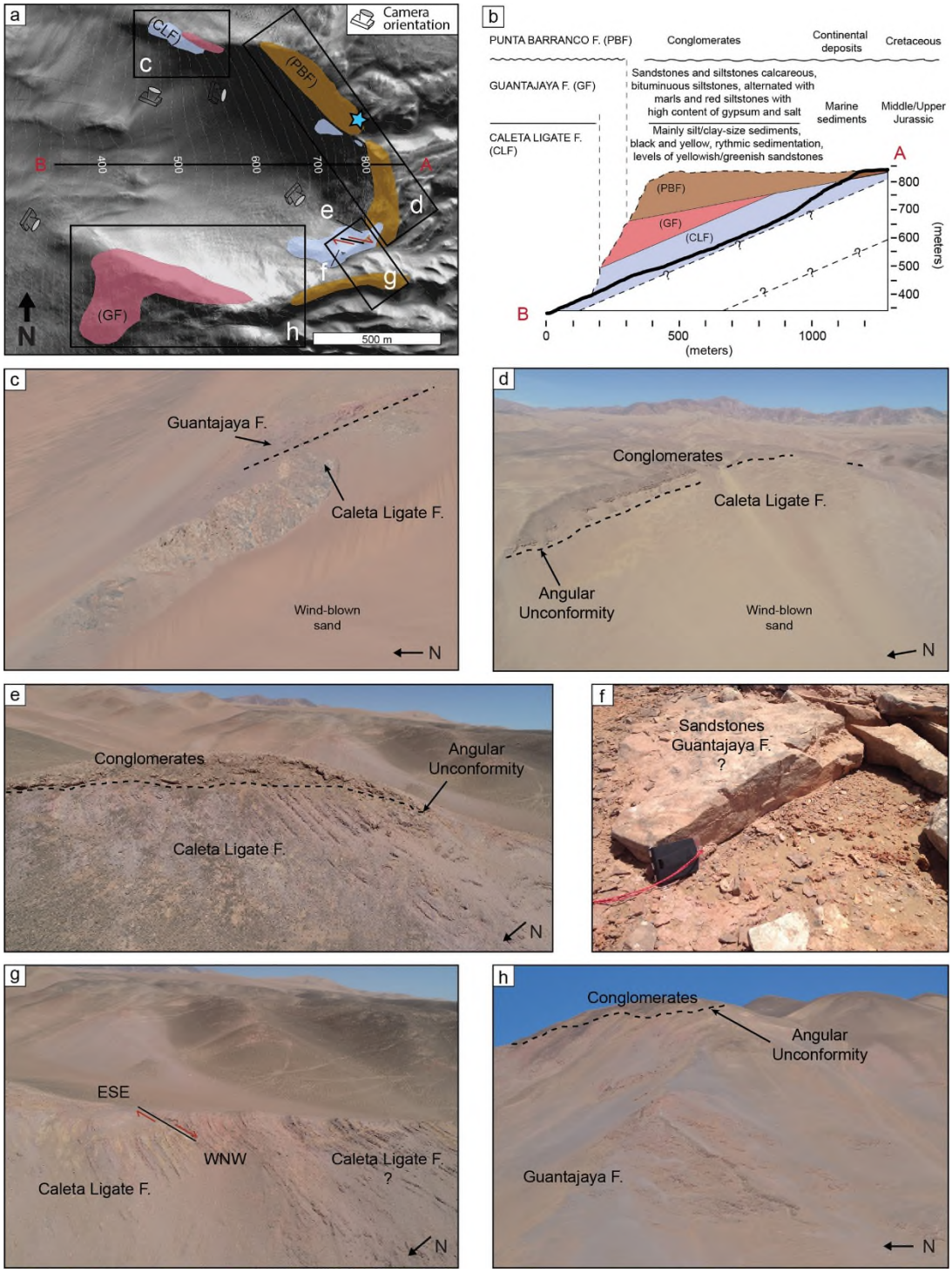

Supplementary Figure S1 - Geological map at the scarp of the El Magnifico landslide. a) Locations at which the lithologies outcrop are shown (coloured patches that follow the classification given in the diagram at the top right); blue star symbol show the location of the outcrop in Supplementary Figure S2. The geological section (b) is made from matching our observations with the formations described and other information provided (such as expected formation thickness) in the Chilean geological map (Novoa, 1970). c-h) annotated drone photos of some of the outcrops.

Supplementary Figure S2 – Conglomerates of the Punta Barranco Formation. This is likely the source lithology of the upper layer brown in colour, matrix-supported, with sub-rounded clasts sizing few centimetres observed at Outcrop 1.

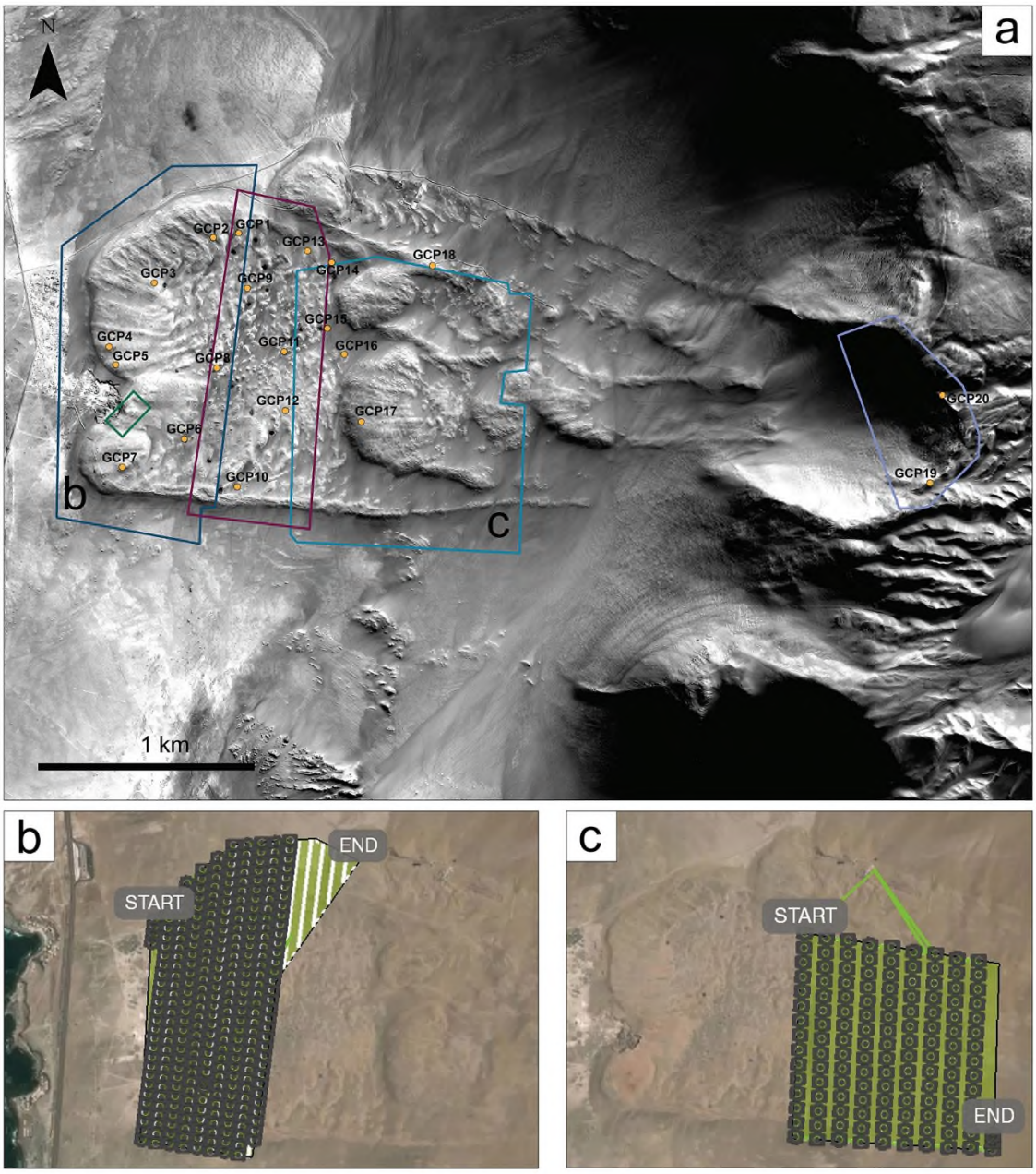

Supplementary Figure S3 – Location of the waypoints used to calibrate drone-derived digital elevation models of the El Magnifico landslide and planned flight missions. a) Orthorectified image derived from Pleiades satellites images. The locations of GCPs is marked on the image with yellow dots. The coloured polygons represent the contour of drone-derived digital elevation models. Dark blue and light blue polygons show the contours of DEMs of the distal and proximal lobes, respectively, used to conduct the morphometric analysis of longitudinal ridges; magenta and violet polygons show the contours of DEMs of the central area of the landslide deposit and part of the head scarp, respectively; b) and c) Flight path and camera positions planned using the 'Pix4D Capture' app to cover the distal lobes and proximal lobes areas, respectively.

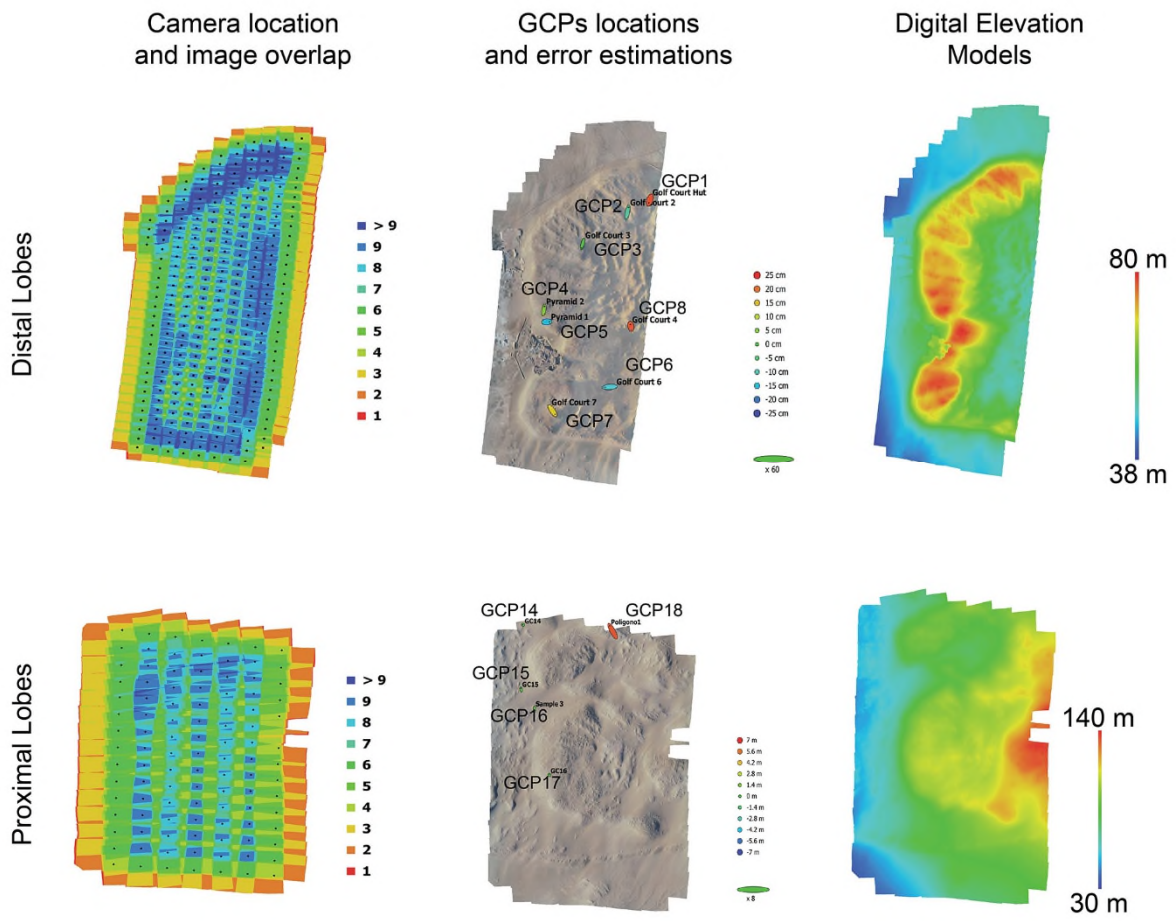

Supplementary Figure S4 – Agisoft Photoscan data report. The figures show the camera locations and image overlap, the Ground Control Points (GCPs) locations and error estimations, and the resulting digital elevation models produced for the distal lobes area and the proximal lobe area.

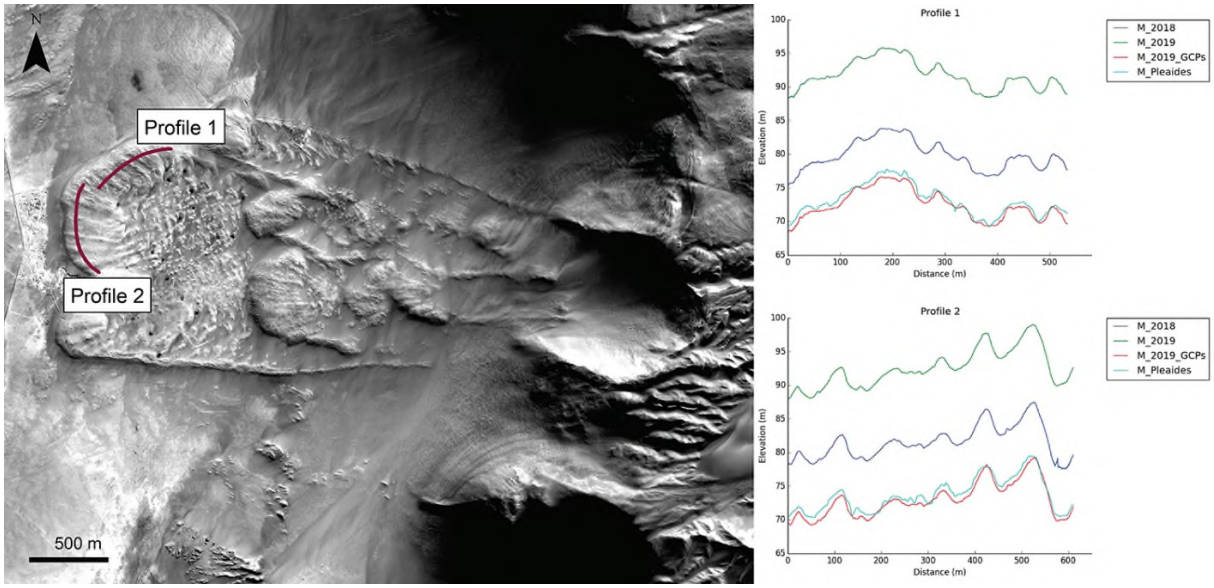

Supplementary Figure S5 – Top image is the orthorectified image deived from Pleiades staellites images. It shows two test profiles along which the topography of the landslide deposit is extracted from 4 different datasets as shown in the two plots below. The dark blue lines corresponds to topography obtained from the drone-derived digital elevation model after 2018 campaign; the green lines corresponds to topography obtained from the drone-derived digital elevation model after 2019 campaign; the light blue lines correspond to the topography obtained from Pleiades stereo-image-derived digital elevation model; the red lines correspond to the topography obtained from the georeferenced 2019 campaign DEM using terrain markers (GCPs) easily identifiable on Pleiades-derived orthoimages. This figure wants to highlight the importance of guarantee consistency when different datasets are used: all the topographic profiles show good qualitative agreement of the features of the topography but having great discrepancy in the elevation data.

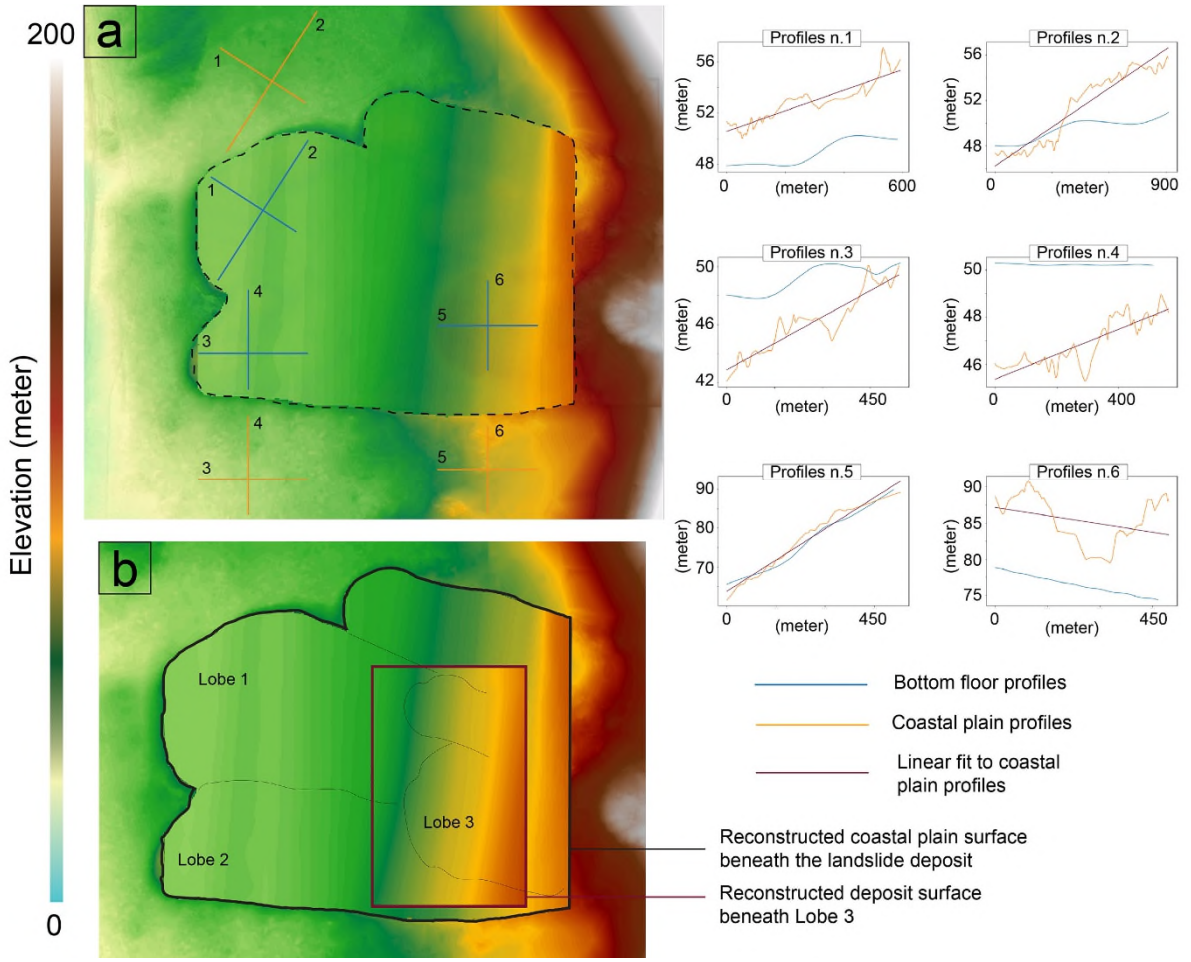

Supplementary Figure S6 – (a) shows the position of the sets of profiles adjacent to the landslide deposit (yellow lines) and within the landslide deposit area (blue lines); within the landslide deposit area (dotted black line) it is shown the reconstructed DEM of the valley floor underneath the landslide deposit as inferred by interpolation of the Pleiades DEM contour lines adjacent the deposit; the sets of profiles are used to generate the plots to the right-hand side of the figure, which show the comparison of the mirror transects (blue and yellow lines 1-6). (b) shows the reconstructed DEM of the coastal plain surface underneath the landslide deposit as inferred by interpolation of the Pleiades DEM contour lines adjacent the deposit (area within black solid line) and the reconstructed DEM of the deposit surface covered by Lobe 3.

Supplementary Figure S7 – Details of Outcrop 1. Close view of thrust structure that forms on the upper part of the megablock; the original beds of the block decrease in height from left to right, forming a wedge; the thrusted and folded part of the megablock is made of bituminous sandstones.

Supplementary Figure 8 – Details of Outcrop 5. Close view of one of the megablocks observed.

Supplementary Figure 9 – Details of Outcrop 1 of well-defined contact between lithologies. Close view of the well-defined contact between the conglomerate-derived upper layer and the grey breccia; note the presence closed to the contact of sub-rounded clasts about 40 cm in size; to the left, clasts of the breccia inject into the conglomerate-derived upper layer. The upper layer is brown in colour, matrix-supported, with sub-rounded clasts sizing few centimetres. The source lithology is likely the conglomerates observed at the scarp (Punta Barranco Formation), although a decrease in the maximum clast size is seemingly present (See Supplementary Material, S2). However, within this brown layer, linear patches of grey clasts appear widespread. The grey clasts are larger than the clasts in the brown part and they appear imbricated at in places.

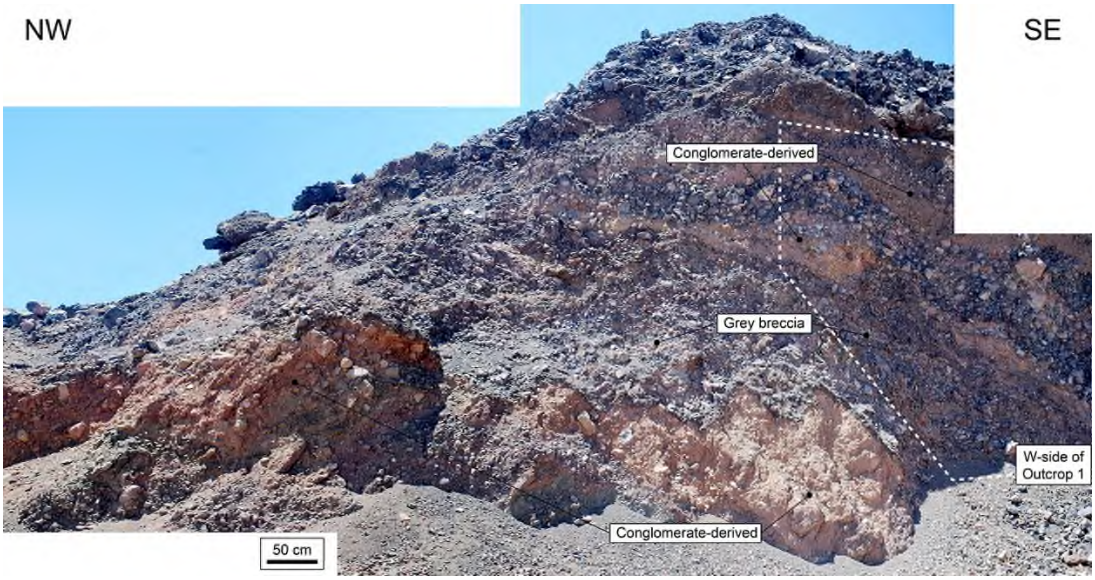

Supplementary Figure 10 – Extended observations near Outcrop 1 reveal the presence a conglomerate-derived layer also below the grey breccia. As it looks, the preservation of the stratigraphic order within rock avalanche deposits often mentioned in the literature does not occur for this case study (other evidence of this are also found at other locations). However, the different lithologies do not mix chaotically, rather they appear to interdigitate.

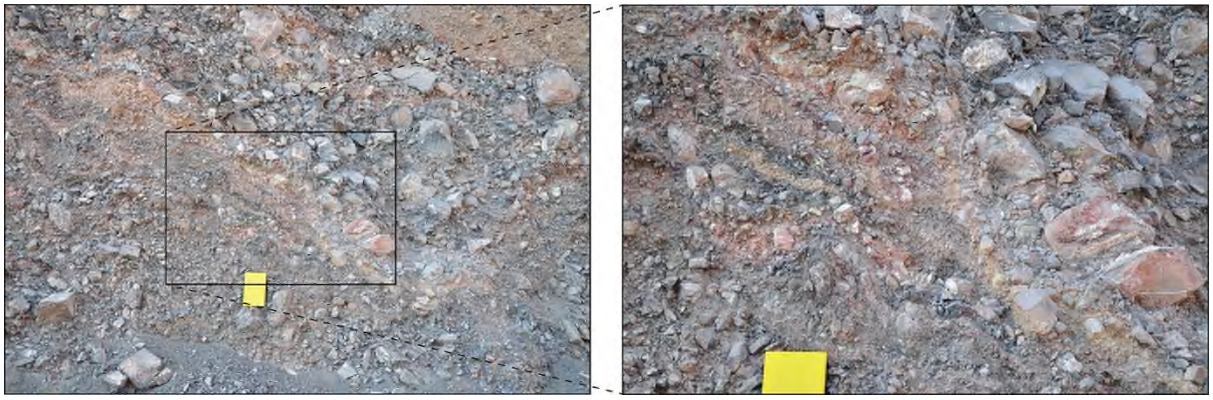

Supplementary Figure 11 – Details of the breccia at Outcrop 1. The breccia is mainly grey in colour, with a lens that appears red, yellow, and greenish in colour. A closer look reveals that clasts similar in size and shape to those of the breccia are within the coloured lens and that they are cemented. This lens dips towards the inner part of the deposit with an angle of about 40° and it has an undulated aspect. The lens separates the grey breccia into two distinct parts: an upper part constituted by dm-size clasts from the lower part constituted by < 10-cm-size clasts; clasts of both parts are closely packed and generally display preferential orientation that mirrors the lens dip.

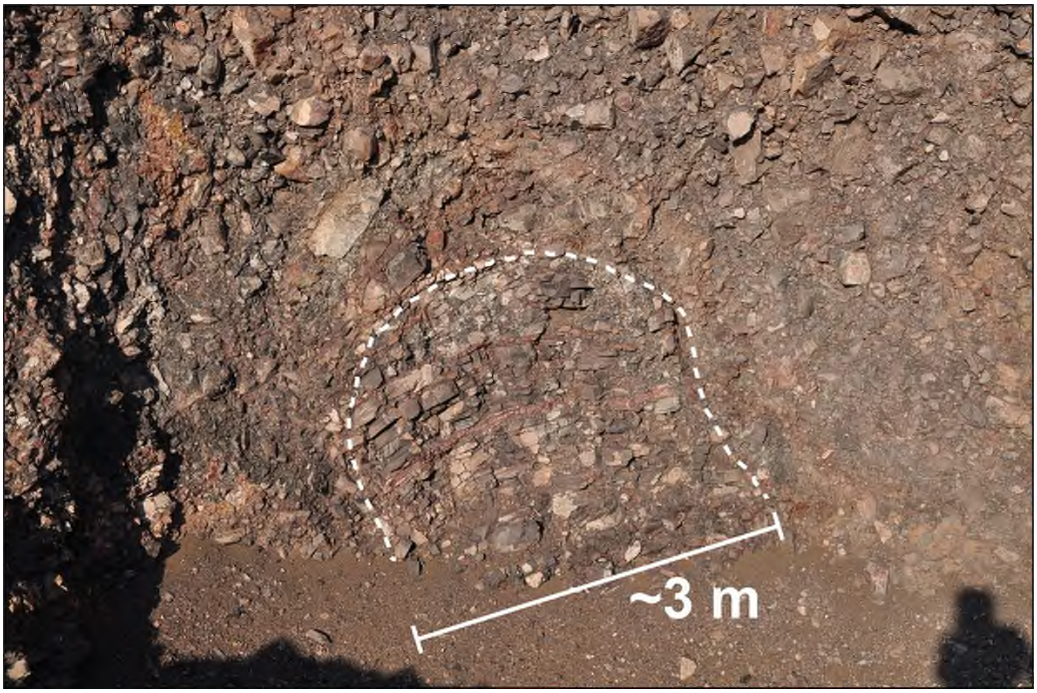

Supplementary Figure 12 - close view of a 3x3 meter block, within the grey breccia, that exhibits well-preserved original bedding planes; the block is formed by the same grey lithology that forms the grey breccia that surrounds it and shows several continuous red layers parallel to the bedding planes.